JOURNAL OF GEOPHYSICAL RESEARCH, VOL. 103, NO. B3, PAGES 5125–5132, MARCH 10, 1998

Experimental observation of fluid flow channels in a single fracture

Stephen Brown

New England Research, White River Junction, Vermont

Arvind Caprihan[1]

Lovelace Respiratory Research Institute, Albuquerque, New Mexico

Robert Hardy

Sandia National Laboratories, Albuquerque, New Mexico

Abstract. A method for obtaining precise replicas of real fracture surfaces using transparent epoxy resins was developed, allowing detailed study of fluid flow paths within a fracture plane. A natural rock fracture was collected from the field and prepared for study. Silicon rubber molds of the fracture surfaces were used to make a transparent epoxy replica of the original fracture. Clear and dyed water were injected into the fracture pore space allowing examination of the flow field. Digitized optical images were used to observe wetting, saturated flow, and drying of the specimen. Nuclear magnetic resonance imaging was used for quantitative measurements of flow velocity. Both video imaging and nuclear magnetic resonance imaging techniques show distinct and strong channeling of the flow at the submillimeter to several-centimeter scale. Each phenomenon, including wetting, drying, dye transport, and velocity channeling, has its own distinct geometric structure and scale. We find that fluid velocities measured simultaneously at various locations in the fracture plane during steady state flow range over several orders of magnitude, with the maximum velocity a factor of 5 higher than the mean velocity. This suggests that flow channeling in fractured rock can cause the breakthrough velocity of contaminants to far exceed the mean flow.

1. Introduction

In terms of fluid flow and transport, rock fractures are commonly described by the parallel plate model, where the fracture surfaces are smooth and parallel. For this geometry, the steady state solution of the Navier-Stokes equations for laminar flow yields the so-called cubic law, where the volumetric flow rate is proportional to the cube of the aperture [e.g., *Iwai*, 1976].

The parallel plate model can only be considered a qualitative description of flow through real fractures. Real fracture surfaces are not smooth parallel plates but are rough and contact each other at discrete points [e.g., *Brown and Scholz*, 1985; *Brown*, 1995]. Fluids and the solutes they contain take tortuous paths when moving through fractures; thus deviations from the parallel plate model are expected. Taking the spatial variation of the aperture into consideration, laminar flow between rough surfaces has been studied theoretically, numerically, and experimentally [e.g., *Iwai*, 1976; *Gangi*, 1978; *Kranz et al.*, 1979; *Brace*, 1980; *Tsang and Witherspoon*, 1981; *Walsh*, 1981; *Stesky*, 1986; *Brown*, 1987; *Pyrak-Nolte et al.*, 1987,1988; *Brown*, 1989; *Zimmerman et al.*, 1991,1992; *Olsson and Brown*, 1993; *Brown et al.*, 1995; *Walsh et al.*, 1997]. These studies confirm that surface roughness plays an important role and can lead to significant departures from the parallel plate model. One of the more interesting processes identified is the restriction of flow to a system of narrow channels within the fracture plane.

A field experiment in the Stripa mine, Sweden [*Bourke*, 1987], demonstrated that flow in a single fracture took place mainly in a few widely separated channels. Five parallel holes were drilled in the fracture plane along the interface between the two contacting fracture surfaces. Each of these holes was pressurized in turn. During these pressurization episodes, various packed-off intervals were monitored for flow. Over a total fracture area of approximately 2×3 m, two large channels comprising about 10% of the sample area were responsible for most of the flow. These channels were separated by approximately 1 m. In a theoretical study of voids and veins formed along rough-walled dilating faults, *Brown and Bruhn* [1996] found that the scale and spacing of channels increases roughly in proportion to the amount of fault slip and could therefore become quite large for an active fault.

[1]Now at New Mexico Resonance, Albuquerque.

Paper number 97JB03542.
0148-0227/98/97JB-03542$09.00

On a much smaller scale, *Pyrak-Nolte et al.* [1987] identified the tortuous geometry of fracture aperture by injecting molten Wood's metal into a single fracture and then opening the fracture when the metal had solidified. *Brown and Scholz* [1985] and *Brown* [1995] studied the topography of many natural rock joint surfaces and computed the aperture. A simple mathematical model of rough surfaces was derived from these data, and the model was used to create realistic simulated apertures. Solutions of fluid flow equations through these simulated fractures show distinct geometry-controlled channeling [*Brown*, 1987,1989; *Thompson and Brown*, 1991].

Channels have been observed on a variety of scales in both the laboratory and in the field. However, many important questions about channeling remain unanswered. The extent to which channels are determined by surface roughness or other factors is not clear. The scaling laws and distribution functions for channel sizes and spacing have not been determined. Also, a generally applicable model of the effect of channeling on the net fracture permeability has not been developed.

In this paper we present laboratory observations of channel structures in a natural fracture under various flow conditions. The purpose of this study was to gain a qualitative understanding of channeling and its complexity to guide the improvement and future development of theoretical models [e.g., *Amadei and Illangasekare*, 1994; *Brown et al.*, 1995; *Yang et al.*, 1995; *Walsh et al.*, 1997].

2. Sample Preparation

A natural fracture in rhyolite was collected from an outcrop near Cerillos, New Mexico. The specimen was trimmed to a rectangular prism, and a silicone rubber mold of each surface of the fracture was then made. The two rubber molds were used to cast transparent epoxy replicas of the original fracture surfaces. The mold-making and casting process for the fracture replicas produces a high-fidelity reproduction of the fracture surfaces at roughness scales from tens of microns to tens of centimeters. Fine details of the roughness are faithfully reproduced on the epoxy replicas, such as tiny structures within the original mineral cleavage surfaces. When the technique was first developed, the quality of the reproduction was checked by comparing surface roughness profiles taken on the original rock and the replicas using the instrument described by *Brown* [1995]. The fine-scale roughness between rock and epoxy cannot be distinguished within the 10-100 μm profilometer errors due to misregistration of each specimen in the instrument and due to electrical and mechanical instrument noise. Through these studies we discovered that long-wavelength features were being introduced in the casts due to bending and stretching of the rubber molds. This problem was remedied in the final process by embedding thick plywood sheets in the rubber mold close to the rough surface during the casting process. The final epoxy replicas were checked for quality of reproduction at long wavelengths by hand fitting them to each other and to the matching rock surface and comparing these to the quality of fit of the two original rock surfaces. After casting, the two epoxy "fracture" surfaces were fitted together and glued into a plastic housing, which contained fluid flow manifolds and pressure seals allowing subsequent water flow and transport experiments to be done.

The specimen was transparent so that light could be transmitted directly across the fracture plane allowing fluid flow processes to be observed with a video camera under a variety of conditions. The specimen was made entirely of plastic which is also transparent to the radio-frequency energy used in nuclear magnetic resonance imaging (NMRI). For both video imaging and NMRI measurements, a peristaltic pump was used to establish steady state flow of water through the specimen. Peristaltic pumps tend to produce a pulsed fluid velocity. We minimized this effect by using several meters of elastic tubing between the pump and the specimen to dampen the flow oscillations within the specimen. In all experiments the fracture plane was kept horizontal, therefore the effects of gravity on flow were negligible.

The final specimen had a length parallel to flow of 12 cm and a width perpendicular to flow of 7.8 cm. A transparent area of approximately 6×6 cm in the fracture plane was available for viewing with the video camera. By monitoring the pressure gradient at several flow rates we estimated the hydraulic aperture from the cubic law to be 148 μm, implying that the cross-sectional area of the fracture available to flow was approximately $7.8 \times 0.0148 = 0.115$ cm^2. The volumetric fluid flow rate was 0.04 cm^3/s for all video imaging experiments and was 0.2 cm^3/s for the NMRI experiments.

3. Video Imaging

A digital video image capture system was used to record images of flow and transport through the fracture replica directly on the computer. This system consisted of a monochrome charge-coupled device (CCD) video camera connected to an image capture board in an industry standard 386 computer. This system had a resolution of 640×480 pixels $\times$ 8 color bits, so that we could resolve fracture images containing 256 gray levels at spatial resolutions of between 0.1-0.2 mm over the 6×6 cm square viewing area. With this equipment, images could be captured and stored at approximately 4 s intervals.

At various times, the water flowing through the fracture was dyed with green food coloring (allowing a maximum effect with the red-sensitive camera). In this way, the absorption of light passing through a liquid containing a dye could be used to derive the two-dimensional aperture distribution and track the motion and dispersion of a solute through the fracture. We took advantage of the Lambert-Beer law [e.g., *Kruyt*, 1952]

$$I_x = I_0 e^{-Kcx}, \tag{1}$$

which states the relationship between the intensity of light I_x passing through a layer of liquid to the thickness x of the layer and the concentration c of the dye. Here I_0 is the intensity of light entering the medium, and K is a material prop-

erty called the extinction coefficient. If K were known, then to derive the thickness x one could simply measure I_x at two arbitrary known values of c. However, for this study we did not know the extinction coefficient, so we were able only to obtain images of the aperture distribution scaled by an arbitrary constant factor. The light intensity for dyed water I_d and plain water I_w was observed at each location in the fracture plane. The argument of the exponential in (1) was solved for at each point as

$$Kcx = -\ln\left(\frac{I_d}{I_w}\right). \tag{2}$$

The normalized aperture, x_{norm}, was then found by dividing this result by its mean value. The aperture distribution derived by this technique for the fractured specimen is shown in Figure 1.

The spatial resolution of this method for measuring the aperture distribution is affected by the contrast between the index of refraction for the epoxy and the fluid. Scattering of light induced by refraction at the solid/liquid interface can blur the image in an unknown way, since some light observed in one pixel may have originated in an adjacent one. This effect will be stronger at regions where the surface slope is high and the fluid film is thick. While it is possible to try to minimize this problem by changing the optical properties of the fluid (by adding sucrose, for example), we chose to only characterize the larger-scale features in the image. We argue that there will be relatively little effect of light scattering if the image is observed at pixel sizes of several times the fluid film thickness. Since the hydraulic aperture was found to be 148 μm, we assume that the aperture image is meaningful at length scales larger than 1-2 mm. Two levels of heterogeneity were found upon close inspection of the aperture distribution (see Figure 1): (1) a single large-scale aperture channel traversing the top of the image from left to right and (2) fine-scale channels traversing the image from upper left to lower right.

3.1. Numerical Simulation of Flow

We wanted to see how the apertures measured in Figure 1 were manifested in the fluid flow. Numerical solutions of the Reynolds equation have been used previously to study flow through rough-walled fractures [*Brown*, 1987,1989; *Zimmerman et al.*, 1991,1992], and we adopted the same method here. The aperture distribution derived from the Lambert-Beer law was reduced in resolution by filtering and resampling to a 64 × 64 pixel grid but kept to the same 6 × 6 cm physical dimensions in the fracture plane. The aperture levels were then offset and scaled to a convenient range for analysis. The Reynolds equation was solved over this aperture mesh by the finite difference method using the same code as *Brown* [1987,1989]. As in Brown's analysis, the boundary conditions were constant pressure boundaries on two opposite sides of the fracture (left and right sides of image) and no flow on the other two sides (top and bottom of image). Figure 1 shows the results of this simulation as images of the vector components of the local volumetric flow rate. Both levels of aperture heterogeneity appear as channels in the flow.

3.2. Wetting

Following the initial aperture measurements, the fracture replica was dried by injection of dry compressed air. Water was then slowly pumped through the dry fracture. Images were taken at various times in this process to observe the wetting front. Example images are shown in Figure 2. Water enters and travels through the fracture first as a fairly blunt finger through the large top channel identified in Figure 1. Air is permanently entrapped in the lower, constricted portion of the fracture. In the general case, the geometry of the initial fingering and the final pattern of entrapped air depends on the water injection pressure, the fluid flow rate, the direction of gravity, and differences in viscosity and density of the invading and displaced fluids. For multiphase flow the wetting angles of the component fluids is an important control

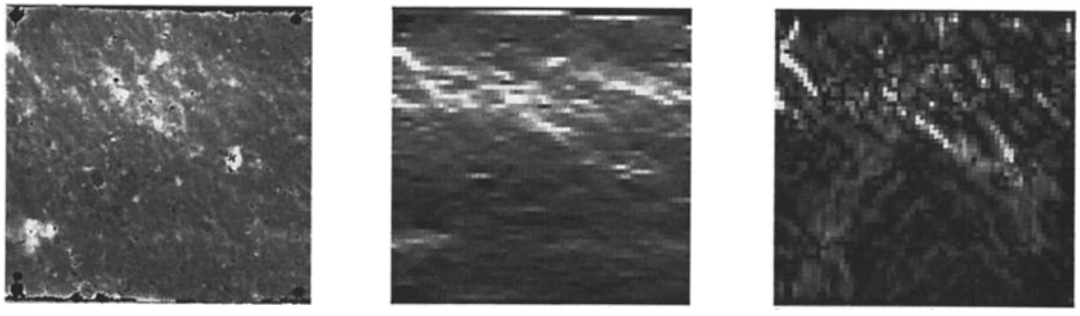

Figure 1. (left) Aperture distribution computed from the Lambert-Beer law. Low to high apertures range from black to white. The circular regions at the corners of the image are fiducial marks spaced on a 6 × 6 cm square. In all subsequent analyses fluid flow was from left to right using this figure as a reference. (middle and right) Volume flow rate distributions calculated from the aperture field on the left using the finite difference model. (middle) Component of volume flow rate parallel to the applied pressure gradient (flow from left to right). (right) Absolute value of the component of volume flow rate perpendicular to the applied pressure gradient.

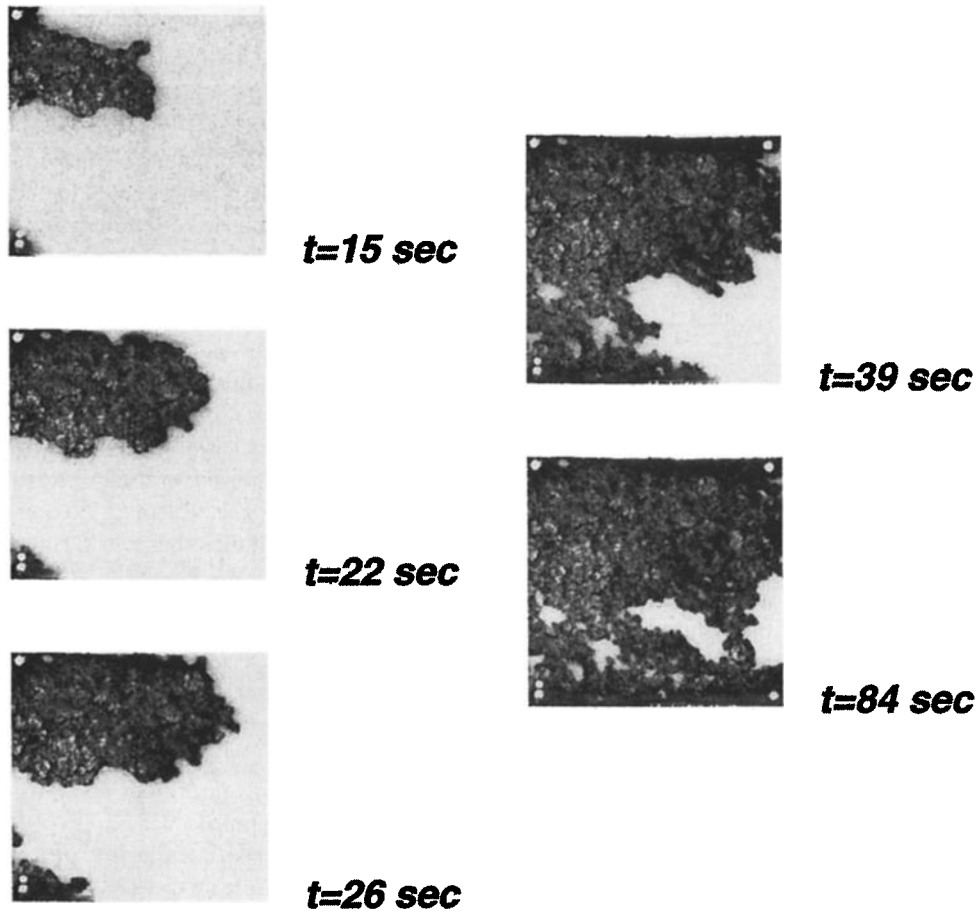

Figure 2. Wetting of the initially dry fracture by water; water entering from the left. Water is a dark shade of gray relative to air. Images are in sequence of increasing time, with labels indicating the time in seconds from the beginning of the test. The bottom-most image on the right approximates the steady state pattern of fluid and entrapped air at this particular flow rate.

on displacement of one fluid by another. Epoxy resins are often quoted to be slightly hydrophobic relative to air. Contrary to this wisdom, we found that the cast rough rock surfaces tended to be slightly hydrophilic, especially when the surfaces had been wet before or the air was humid. However, since we could not control the surface conditions within the assembled specimen, we could not estimate the precise wetting angle during these experiments. Fluid flow rates were high enough that evaporation was not important in determining the fluid/air interface during these experiments.

3.3. Dye Transport

After the wetting experiment, the remaining air in the fracture was expelled, and the fracture was saturated with clear water. Steady state flow of water was established. An image was taken of the water-saturated fracture. Green food color dye was injected into the upstream end of the flow system, and a series of images were taken to observe the transport of the dye through the fracture (Figure 3). The dye entered the viewing area in the large-scale aperture channel first, then at a later time appeared in the lower constricted-aperture region. Eventually, the dye flushed clear of the large channel but remained in the constricted region for an extended period of time. The dye flow experiment emphasizes the mechanism for the broad tail of the solute breakthrough curve discussed by *Thompson* [1991] and *Thompson and Brown* [1991], where diffusion can be a significant process of dispersion relative to advection for slow flow through a variable aperture fracture. The experiments also show the complex and broad range of scales in the channel structure. The fine-scale channels seen for dye transport were not manifested in the wetting behavior due to surface tension effects. Figure 4 shows an example cross section of the channels at a particular time in the evolution of the transport of dye through the fracture. The geometry of the dye channels depends on the imposed flow velocity and the interplay between advection and diffusion processes.

A parameter of some importance in studying channel geometry is the tortuosity of a flow path [e.g., *Brown*, 1989]. The concept of tortuosity arises in studies of flow in porous media, where the complex pore geometry is replaced by an "equivalent channel model" consisting of a distribution of tubes with idealized cross-sectional shapes. *Brown* [1989] discusses how the equivalent channel model of *Paterson*

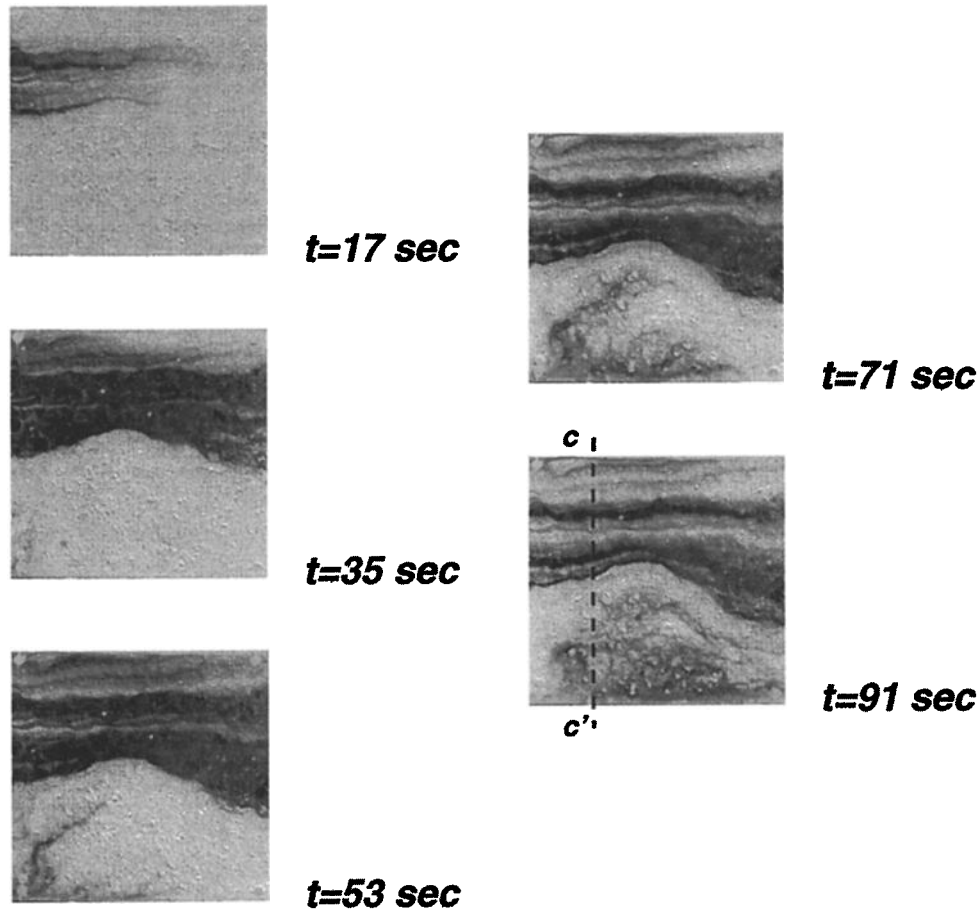

Figure 3. Transport of dye into the water-saturated fracture with steady state fluid flow; dye and water entering from the left. Increasing dye concentration is indicated by darker shades of gray relative to clear water. Images are in sequence of increasing time, with labels indicating the time in seconds from the beginning of the test.

[1983] and *Walsh and Brace* [1984] relates to flow and transport in fractures. In this model the permeability k is related to the equivalent channel geometry as

$$k = \frac{m^2}{b}\frac{\phi}{\tau^2}, \tag{3}$$

where m is the hydraulic radius (= 1/2 of the tube radius for cylindrical tubes, = 1/2 of the surface separation for parallel plates), b is the shape factor (= 2 for cylindrical tubes, = 3 for parallel plates), ϕ is the porosity, and τ^2 is the tortuosity. The tortuosity parameter is defined as $\tau = \Delta l/\Delta x$, where Δl is the actual length of a streamline and Δx is the nominal travel distance parallel to the direction of macroscopic flow. *Brown* [1989] points out that tortuosity values for viscous fluid flow should be different than the tortuosity value used for conduction of electric current. *Brown* [1989] found that various simulations of fluid flow through simulated fractal fractures had average tortuosity parameters approximately in the range $1 < \tau < 2$ depending on the separation of the fracture surfaces. For our experiments we estimated the tortuosities at selected locations by measuring the length of streamlines at time $t = 91$ s (Figures 3 and 4). The measurement was made by tracing over each streamline by eye with a computer-aided digitizing program, then computing the line length by integration of the infinitesimal line segments. The types of errors encountered in this technique provides us approximately with a lower-bound for the tortuosity. Consistent with the results of *Brown* [1989], we observed values in the range $1.05 \leq \tau \leq 1.37$ for flow in our specimen (Figure 4). Since the permeability depends on τ^2, then these results imply that fracture permeability predictions could be in error by a factor in the range of 2–4 if the parallel plate model was used without considering the surface roughness.

3.4. Drying

While remaining under steady state flow conditions, the dye was flushed out of the fracture and the supply of water was replaced by dry air. A series of images was taken to observe the initial part of the drying process (Figure 5). As air enters the fracture, it initially breaks into a series of bubbles which move separately at first, then coalesce to form a continuous air-filled pathway across the fracture. The tendency of the air to break into bubbles during flow confirms

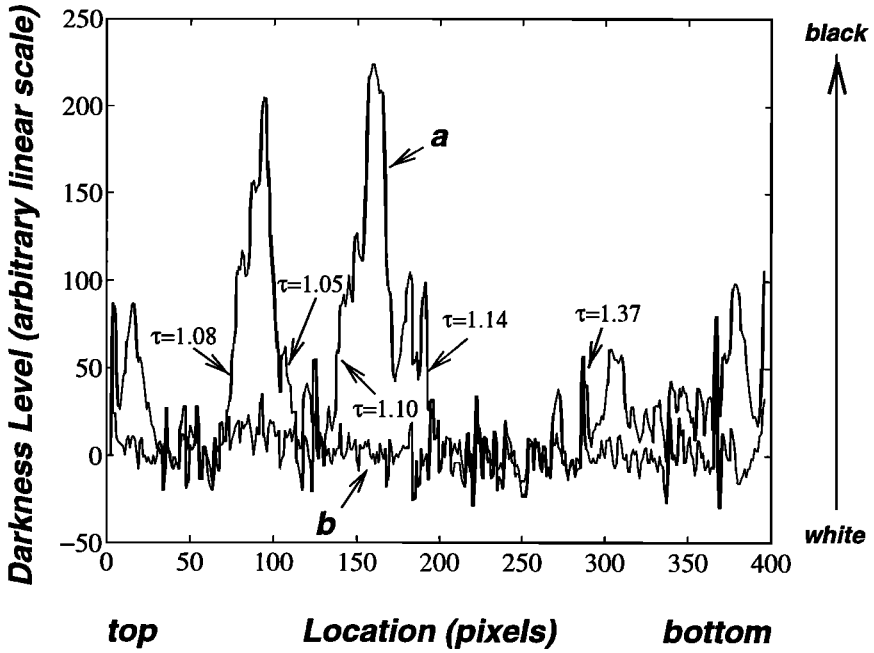

Figure 4. Dye concentration channels. Profiles represent the darkness level ranging from white to black with 256 shades of gray. Profile a is from top to bottom along section c-c' of Figure 3 at time $t = 91$ s. Profile b is the background level from the same location when only clear water is present before dye injection. The spikes in profile a indicate areas of large quantities of dye (large light extinction) and thus mark the location and size of channel structures in the dye transport. The tortuosity parameter τ was measured for several streamlines crossing this profile (the locations of the measured streamlines and the tortuosity values are indicated).

the water-wet character of the fracture surfaces. Significant amounts of trapped water remain. The dominant airflow pathway follows the large aperture channel identified in Figure 1, and the trapped water resides in the low-aperture regions identified earlier. The geometry of the air fingers is different from the water fingers observed during the wetting process. Again, the geometry of the initial fingering and the final pattern of entrapped water depends on the air injection pressure, the fluid flow rate, the direction of gravity, differences in viscosity and density of the invading and displaced fluids, and the wetting angle of water relative to air. Fluid flow rates were high enough that evaporation was not important in determining the fluid/air interface during these experiments.

4. Nuclear Magnetic Resonance Imaging

Pulsed nuclear magnetic resonance imaging was used to observe the flow in this laboratory specimen. The technique used is described in detail by *Caprihan and Fukushima* [1990]. NMRI is a noninvasive method that derives its signal by exciting the nuclear magnetic moments in the sample by radio frequency magnetic field pulses. It can obtain hydrodynamic parameters of flows including the fluid velocity vector field. In this type of experiment we monitor the signal only from the protons in the liquid flowing in the specimen. The fracture was saturated with tap water, and a steady state flow experiment was performed. The fluid velocity vector field was measured from the phase field of the magnetization, which was sensitized to the velocity by bipolar magnetic field gradient pulses. Two sets of experiments yielded the two components of velocity in the fracture plane. The component of the velocity distribution parallel to the macroscopic flow as measured quantitatively by NMRI is shown in Figure 6. The large high-velocity channel seen at the top of this image coincides with the prominent aperture channel identified earlier. However, a simple rescaling of the color map reveals many smaller-scale velocity channels superimposed on this large-channel structure. The probability distribution of the measured velocities is broad, somewhat bimodal, and ranges over many orders of magnitude. The mean velocity within this region was found to be 3.2 cm/s and the maximum velocity was 18.3 cm/s. It is not known at this time whether the negative velocities appearing in Figure 6 are real, but it is conceiveable that there is a small fraction of the area with reversed flow along extremely tortuous paths.

5. Discussion

Using two techniques, digitized optical imaging and nuclear magnetic resonance imaging, we have observed fluid flow through a natural rock fracture specimen under a variety of conditions. During these experiments we observed channeling of flow at submillimeter to several-centimeter scales.

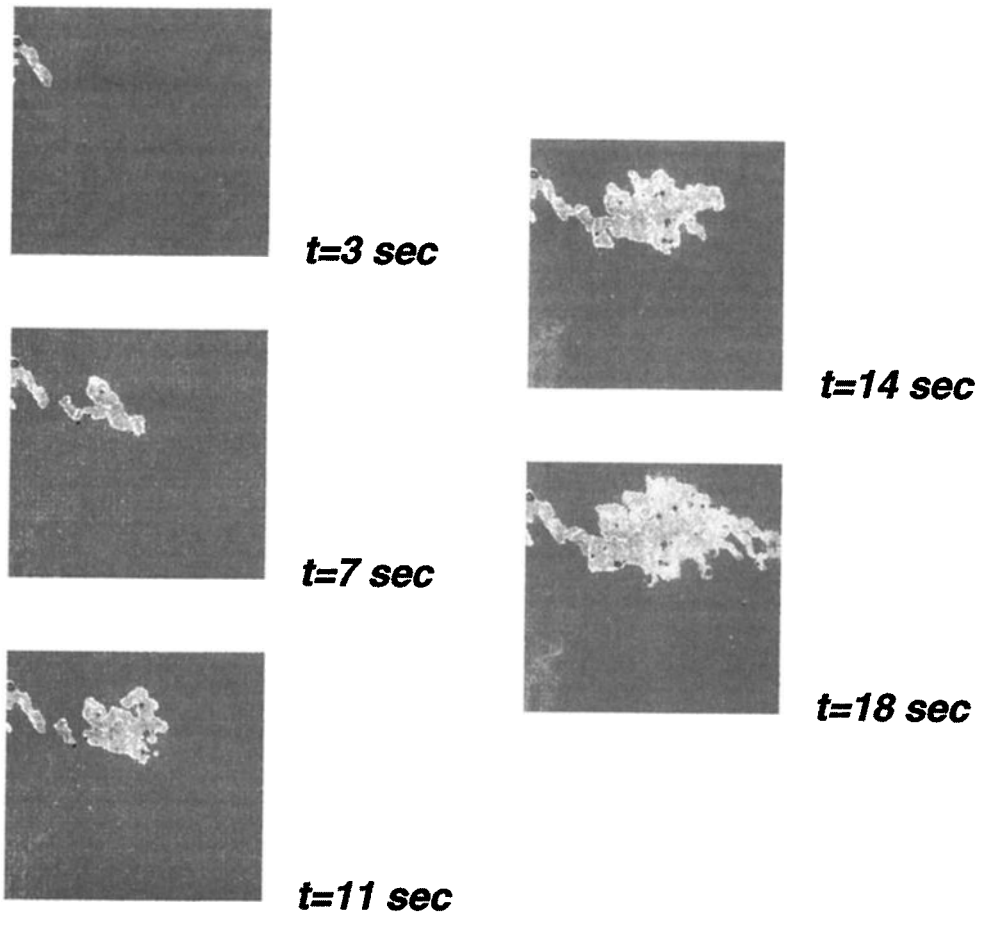

Figure 5. Air invasion into the initially water-saturated fracture; air entering from the left. Air is a light shade of gray relative to water. Images are in sequence of increasing time, with labels indicating the time in seconds from the beginning of the test.

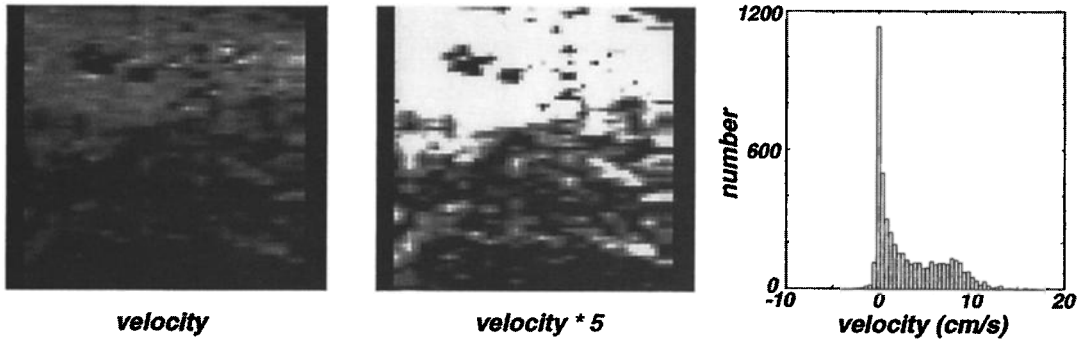

Figure 6. (left) Velocity distribution in the fracture (component parallel to macroscopic flow) measured by NMRI. Low to high velocities range from black to white. The region displayed just fills the 6 × 6 cm square region defined by the fiducial marks visible in Figure 1. A velocity measurement was made within each 0.833 × 0.8 mm pixel. (middle) Velocity distribution with a new color map (velocities scaled by a factor of 5) to emphasize some of the smaller-scale channels. (right) Histogram of velocities in the fracture plane in units of cm/s.

Each phenomenon, including wetting and drying fronts, dye transport, and flow velocity distributions, has its own distinct characteristics. We found that channels have complex geometries and a wide range of scales. Channeling of flow is an important issue in determining the residence time and breakthrough of contaminants traveling through fractured media. Of particular relevance, for example, we found a spread of several orders of magnitude in fluid velocities, with the maximum velocity a factor of 5 higher than the mean velocity. Due to channeling, then, the breakthrough velocity of contaminants can far exceed the mean flow.

Channeling is expected in fractures, since the apertures have short-range spatial correlation. Large aperture regions therefore tend to persist and can be thought of as forming an interconnected set of tube-like structures through which fluid can flow. However, these aperture channels do not by themselves define the geometry of all types of flow channels. Each physical phenomenon, such as wetting, drying, saturated flow, and solute transport has additional physical constraints or boundary conditions. The net result is that the geometry of the various flow channels depends on the physical process.

Acknowledgments. This work was supported by the U.S. Department of Energy, Office of Basic Energy Sciences, Geosciences Research Program under contract DE-AC04-94AL85000 to Sandia National Laboratories. Experiments were performed at the Geomechanics Laboratory at Sandia National Laboratories, Albuquerque, New Mexico, and at the NMR Laboratory of the Lovelace Respiratory Research Institute, Albuquerque, New Mexico. Some of the work by S. Brown was performed while he was an employee of Applied Research Associates, South Royalton, Vermont.

References

Amadei, B., and T. Illangasekare, A mathematical model for flow and solute transport in non-homogeneous rock fractures, *Int. J. Rock Mech. Min. Sci. Geomech. Abstr., 31*, 719-731, 1994.

Bourke, P.J., Channeling of flow through fractures in rock, in *Proceedings of GEOVAL-87*, pp. 167-177, Swed. Nucl.Power Insp., Stockholm, 1987.

Brace, W.F., Permeability of crystalline and argillaceous rocks, *Int. J. Rock Mech. Min. Sci. Geomech. Abstr., 17*, 241-251, 1980.

Brown, S.R., Fluid flow through rock joints: The effect of surface roughness, *J. Geophys. Res., 92*, 1337-1347, 1987.

Brown, S.R., Transport of fluid and electric current through a single fracture, *J. Geophys. Res., 94*, 9429-9438, 1989.

Brown, S.R., Simple mathematical model of a rough fracture, *J. Geophys. Res., 100*, 5941-5952, 1995.

Brown, S.R., and R.L. Bruhn, Formation of voids and veins during faulting, *J. Struct. Geol, 18*, 657-671, 1996.

Brown, S.R., and C.H. Scholz, Broad bandwidth study of the topography of natural rock surfaces, *J. Geophys. Res., 90*, 12575-12582, 1985.

Brown, S.R., H.W. Stockman, and S.J. Reeves, Applicability of the Reynolds equation for modeling fluid flow between rough surfaces, *Geophys. Res. Lett., 22*, 2537-2540, 1995.

Caprihan, A., and E. Fukushima, Flow measurements by NMR, *Phys. Rep., 198*, 195-235, 1990.

Gangi, A.F., Variation of whole and fractured porous rock permeability with confining pressure, *Int. J. Rock Mech. Min. Sci. Geomech. Abstr., 15*, 249-257, 1978.

Glass, R.J. and M.J. Nicholl, Quantitative visualization of entrapped phase dissolution within a horizontal flowing fracture, *Geophys. Res. Lett., 22*, 1413-1416, 1995.

Iwai, K., Fundamental studies of fluid flow through a single fracture, Ph.D. thesis, Univ. of Calif., Berkeley, 1976.

Kranz, R.L., A.D. Frankel, T. Engelder, and C.H. Scholz, The permeability of whole and jointed Barre granite, *Int. J. Rock Mech. Min. Sci. Geomech. Abstr., 16*, 225-234, 1979.

Kruyt, H.R., *Colloid Science, Vol. 1, Irreversible Systems*, Elsevier, New York, 1952.

Olsson, W.A., and S.R. Brown, Hydromechanical response of a fracture undergoing compression and shear, *Int. J. Rock Mech. Min. Sci. Geomech. Abstr., 30*, 845-851, 1993.

Paterson, M.S., The equivalent channel model for permeability and resistivity in fluid-saturated rocks: A reappraisal, *Mech. Mater., 2*(4), 345-352, 1983.

Pyrak-Nolte, L.J., L.R. Myer, N.G.W. Cook, and P.A. Witherspoon, Hydraulic and mechanical properties of natural fractures in low permeability rock, in *Proceedings of the Sixth International Congress on Rock Mechanics*, edited by G. Herget and S. Vongpaisal, pp. 225-231, A. A. Balkema, Brookfield, Vt., 1987.

Pyrak-Nolte, L.J., N.G.W. Cook, and D.D. Nolte, Fluid percolation through single fractures, *Geophys. Res. Lett., 15*, 1247-1250, 1988.

Stesky, R.M., Electrical conductivity of brine-saturated fractured rock, *Geophysics, 51*, 1585-1593, 1986.

Thompson, M.E., Numerical simulation of solute transport in rough fractures, *J. Geophys. Res., 96*, 4157-4166, 1991.

Thompson, M.E., and S.R. Brown, The effect of anisotropic surface roughness on flow and transport in fractures, *J. Geophys. Res., 96*, 21923-21932, 1991.

Tsang, Y.W., and P.A. Witherspoon, Hydromechanical behavior of a deformable rock fracture subject to normal stress, *J. Geophys. Res., 86*, 9287-9298, 1981.

Walsh, J.B., Effect of pore pressure and confining pressure on fracture permeability, *Int. J. Rock Mech. Min. Sci. Geomech. Abstr., 18*, 429-435, 1981.

Walsh, J.B., and W.F. Brace, The effect of pressure on porosity and the transport properties of rock, *J. Geophys. Res., 89*, 9425-9431, 1984.

Walsh, J.B., S.R. Brown, and W.B. Durham, Effective media theory with spatial correlation for flow in a fracture, *J. Geophys. Res., 102*, 22587-22594, 1997.

Yang, G., S.R. Brown, L.R. Myer, and N.G.W. Cook, Microscopic analysis of macroscopic transport properties of single natural fractures using graph theory algorithms, *Geophys. Res. Lett., 22*, 1429-1432, 1995.

Zimmerman, R.W., S. Kumar, and G.S. Bodvarsson, Lubrication theory analysis of the permeability of rough-walled fractures, *Int. J. Rock Mech. Min. Sci. Geomech. Abstr., 28*, 325-331, 1991.

Zimmerman, R.W., D.-W. Chen, and N.G.W. Cook, The effect of contact area on the permeability of fractures, *J. Hydrol., 139*, 79-96, 1992.

S. Brown, New England Research, 76 Olcott Drive, White River Junction, VT 05001. (email: sbrown@ner.com)

A. Caprihan, New Mexico Resonance, 2425 Ridgecrest Dr. SE, Albuquerque, NM 87108. (email: acapriha@lucy.lrri.org)

R. Hardy, Geomechanics Dept., MS-0751, Sandia National Laboratories, Albuquerque, NM 87185. (email: rdhardy@sandia.gov)

(Received May 1, 1997; revised November 4, 1997;
accepted December 3, 1997.)